IEEE Access
Multidisciplinary | Rapid Review | Open Access Journal

SPECIAL SECTION ON GREEN INTERNET OF THINGS

Received November 19, 2019, accepted December 16, 2019, date of publication December 20, 2019,
date of current version December 31, 2019.

Digital Object Identifier 10.1109/ACCESS.2019.2961152

Dynamic and Non-Centric Networking Approach Using Virtual Gateway Platforms for Low Power Wide Area Systems

OU ZHAO, (Member, IEEE), WEI-SHUN LIAO, (Member, IEEE), KENTARO ISHIZU, (Member, IEEE), AND FUMIHIDE KOJIMA, (Member, IEEE)

Wireless Networks Research Center, National Institute of Information and Communications Technology, Yokosuka 239-0847, Japan

Corresponding author: Ou Zhao (zhaoou@nict.go.jp)

This work was supported by the Ministry of Internal Affairs and Communications, Japan, through the Research and Development Contract for the Expansion of Radio Wave Resources.

ABSTRACT To actively develop and promote Internet of Things related techniques, we propose a dynamic and non-centric networking approach using virtual gateway platforms, and evaluate it based on low-power wide-area networks that adopt the traditional star and mesh topologies. In our approach, for each local device, we first present a device management method in which two working modes are set to indicate whether the device works as a virtual gateway (VGW) or provides relay services. Then an internal parameter is defined to manage the mode by considering the device's current states, such as battery power remaining, presence or absence of an external power supply, etc. We thereafter propose a mode switching method where two time-varying threshold values are configured and help a local device to switch between the two modes through the use of an internal parameter. Finally, a path determination algorithm is applied to find routes for data transmission with or without devices playing the role of VGWs. Computer simulation results indicate that the proposed networking approach can take advantage of both traditional star and mesh systems, enables dynamic and non-centric changes in network configurations, and finally ensures that in most cases, the transmission performance is equivalent to or better than that of other network setups.

INDEX TERMS Internet of Things (IoT), mesh networks, network topology, low-power wide-area (LPWA), multi-hop, Wi-SUN, virtual gateway, decentralization.

I. INTRODUCTION

A. TECHNICAL BACKGROUND

In recent years, as the number of things in Internet of Things (IoT) systems has grown, data transmissions among things has become increasingly complex, and the balance between communication demands and infrastructure costs is thus being emphasized [1]–[3]. In contrast to existing short range wireless communication technologies including Bluetooth and Wi-Fi, low-power wide-area (LPWA) networking technology that is designed to allow long range communications at a low bit rate among connected objects, has emerged and attracted increasing attention [4]–[10].

There are a number of competing standards and vendors in the LPWA network space, such as Long Range (LoRa) digital wireless data communication technology[1] and wireless smart utility network (Wi-SUN) communication systems[2]. The latest experiments show that based on one hop in a LoRa physical layer (PHY) wide area network, the so-called LoRaWAN with star topology can transmit data approximately 15 km in an open area [11], [12]. Similarly, a mesh topology based Wi-SUN field area network (FAN), which enables devices to have multiple connections to those around them, can also create large-scale wireless communication networks with multiple hops. However, owing to obstacles between devices and co-channel interference that attenuate desired wireless signal strength and result in bit errors in realistic wireless environments [13], [14], how to improve the data rate while

The associate editor coordinating the review of this manuscript and approving it for publication was Haris Pervaiz.

[1]https://lora-alliance.org
[2]https://www.wi-sun.org

expanding the coverage area as far as possible for LPWA networks is still an open issue [15].

Unfortunately, it is not possible to meet both goals simultaneously while providing high-quality service. Colloquially speaking, in LoRaWAN, changing the spreading factor (SF) to the maximum (default is 12) and thus improving the receiver sensitivity can considerably extend the communication range [16]. However, the use of a larger SF decreases the bit rate and increases time on air[3], so ensuring higher speed transmission in LoRaWAN is difficult, as a higher number of data collisions may occur. Likewise, in Wi-SUN FAN, although more devices are under control through long hop forwarding, higher latency and lower rates tend to reduce the quality of service [7]. To solve these issues, researchers suggest deploying more gateways to decrease average access distance and to improve the data rate without range reduction [6], [17]–[19]. However, this solution obviously increases the cost of the network and the system complexity.

B. RELATED STUDIES

Carrying out a general survey of studies involving IoT technology published over the past several years, we found that some up to date studies have focused on the star topology using LoRaWAN with dense device deployment and multiple gateways [17]–[19]. Specifically, in [17], the authors employed gateways with multiple receiving antennas to achieve spatial diversity and evaluated the performance through theoretical analysis and computer simulations. Their results show that the use of multiple receiving antennas in gateways is always beneficial for LoRaWAN. In [18], a scalability analysis of the above-mentioned LoRaWAN was performed in an ns-3 module that enables the study of multiple-gateway networks with thousands of devices. An adaptive data rate mechanism to configure the communication parameters of LoRaWANs was proposed and evaluated in [19]. Although the analysis results agree that increasing gateway density can ameliorate transmission performance issues, experimental support is lacking, thereby making it difficult to apply a system in practice owing to the network size and associated deployment cost, for example.

On the other hand, drawing on past experience with Wi-SUN FANs, partial research studies such as those in [20]–[22] suggest employing a mesh topology based network structure instead of the traditional star topology. In particular, the authors in [21], [22] provided a detailed discussion regarding LoRa mesh networking and evaluated its performance through real-world experiments. Their results indicated that the mesh topology approach is one feasible solution to increase the communication range and packet delivery ratio without the need to install additional gateways in LPWA networks.

Generally, the data relay, as the core of a mesh network structure, is not only associated with IoT related technical fields, it has also been actively and widely discussed regarding user cooperation mechanisms proposed for cellular communication [23]–[28], and currently, issues concerning energy consumption need to be clarified and addressed [26], [27]. In brief, the authors in [26] mathematically analyzed the energy consumption of mobile terminals in cellular networks with the use of data relays, and indicated that power consumption can be reduced by dynamically selecting a terminal with the best channel condition as an aggregator and then relaying data through it. The literature [27] further confirmed these results via a field experiment using a smart phone test-bed. However, as other articles have pointed out, terminals that take responsibility for relaying data may use more energy and thus, in extreme cases, unexpectedly lose power. Additionally, it is often assumed that such types of terminals are always willing to relay data, which may not always be true or optimal. These are also common problems encountered in battery-powered IoT devices.

In fact, several reasonable power consumption algorithms described in [28] have been presented recently for mobile terminals. The algorithms actually involve a tradeoff between the consumed energy and the data rate, and are designed for centralized network structures in which a base station (BS) needs to collect positions, channel state information, as well as battery power remaining for all mobile terminals, and then controls all transmissions based on the above uploaded information. From the viewpoints of transmission efficiency and implementation, unfortunately, these methods are not very suitable for the low bit rates associated with LPWA systems.

C. OUR CONTRIBUTION

Motivated by the previous studies and in an attempt to break away from the traditional gateway or BS centric transmission scenarios, we propose a dynamic and non-centric networking approach and apply it to LPWA systems. The core of the proposal is that a time-varying (in the general case) parameter is embedded in each local device and helps the device to decide whether to provide relay services according to its current states, such as availability of an external power supply[4], battery power remaining, subjective requirements related to network performance, and so on. Basically, the proposed method can dynamically create a network with either star or mesh topology, or can enable an extraordinary network configuration that adopts the characteristics of both the traditional star and mesh network features; for instance, by balancing energy consumption among devices while maintaining system throughput at an acceptable level.

[3] A longer time on air usually means that a radio module needs more time to send the same amount of data, and leads to a higher probability of data collisions.

[4] The external power supply is defined as a traditional alternating/direct-current power source, or other devices that supply electric power via photovoltaic modules.

Moreover, using the concepts of decentralization[5] [29]–[31], it is unnecessary for central controllers, i.e., gateways or BSs, to know all device information and control all transmission processes. Partial tasks such as determining whether to provide relay services is performed by the local devices themselves. Therefore, saving bandwidth resources and improving communication efficiency is possible under this scenario. In addition, we currently promote the proposal on LPWA networks using IoT devices, but it can also be widely adopted by other wireless communication systems where a data relay or forwarding strategy is strongly recommended.

The remainder of this paper is organized as follows. In Sect. II, we describe the system architecture under the considerations discussed previously and explain the proposed networking approach in greater detail. In Sect. III, details regarding the employed channel models are provided and a suitable channel access method is introduced to evaluate the proposal. In Sect. IV, we present and analyze simulated results and summarize the key findings. Discussions are provided in Sect. V, and concluding remarks are presented in Sect. VI.

Notations: We use upper-case boldface, lower-case boldface, and calligraphic font to denote matrices, vectors, and integer collections, respectively. The size of a collection $\mathcal{A}$ is indicated by $|\mathcal{A}|$, and $\mathbb{C}^{m\times n}$ and $\mathbb{R}^{m\times n}$ denote the $m \times n$ dimensional complex and real matrix space. The sub-matrix constructed by extracting the collection of rows $\mathcal{R}$ and collection of columns $\mathcal{C}$ from a matrix $\boldsymbol{A}$ is denoted by $[\boldsymbol{A}]_{\mathcal{R},\mathcal{C}}$. We use "$\circ$" to denote the Hadamard product, i.e., $[\boldsymbol{A}\circ\boldsymbol{B}]_{i,j} = [\boldsymbol{A}]_{i,j}[\boldsymbol{B}]_{i,j}$. To distinguish the νth power of a matrix $\boldsymbol{A}^{\nu}$, we use $\boldsymbol{A}^{\nu\circ}$ to denote the νth power of $\boldsymbol{A}$ with respect to the Hadamard product such that $\boldsymbol{A}^{\nu\circ}\circ\boldsymbol{A}^{-\nu\circ} = \boldsymbol{I}$, where $\nu \in \mathbb{R}$ and $\boldsymbol{I}$ is the identity matrix.

II. SYSTEM ARCHITECTURE

We consider a common wireless communication system in which a gateway (or BS) and $|\mathcal{U}|$ ($\mathcal{U} := \{1, \cdots, U\}$ indexed with u) devices are uniformly distributed in a coverage area. For simplicity, both the gateway and devices are equipped with a single antenna, and uplink data transmission is the major factor to be taken into consideration. A wired connection network server is deployed for the system, which performs mathematical calculations, accepts upstream packets, and sends downstream traffic to devices through the gateway. An illustration of device and gateway deployments for the considered system is presented in Fig. 1.

In the present study, the devices and gateway deployed in the coverage area can create three types of networks: the traditional star and mesh topologies [32], and the proposal. The star topology network adopted is one where every device is directly connected to the gateway without data forwarding. The traditional mesh network is a full mesh topology network in which every device has a connection to each of the other devices in the network. The proposed networking approach consists of three components: a device management method, mode switching method, and path determination algorithm. We provide their details in the following subsections.

[5]Concepts of decentralization have been applied widely in many fields such as blockchains [31]. A more detailed description can be found in [29], [30].

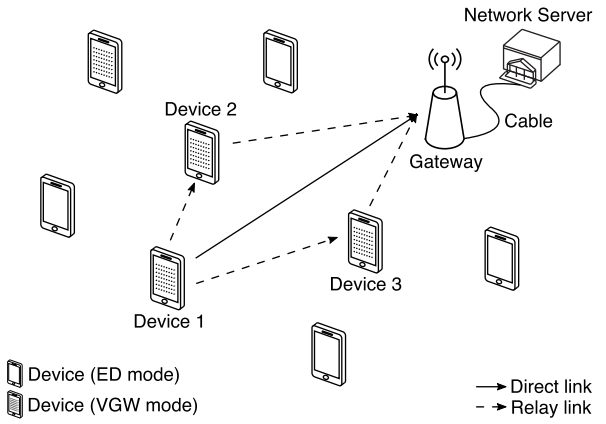

FIGURE 1. Illustration of device and gateway deployments for The wireless communication system considered in this study.

A. DEVICE MANAGEMENT METHOD

We configure each device in the proposed networking approach so that it can and must independently work in one of two modes; one is called the end-device (ED) mode and the other is a customized mode called the virtual gateway (VGW) mode. Currently, a device that operates in the ED mode is considered as a typical device which only transmits its own data; and a device working in the VGW mode is given two tasks: sending its own data, and relaying data received from other devices. A mode switching method embedded in each device can dynamically determine which mode should be activated and is described in the next subsection.

In our proposal, an internal and time-varying parameter named the "point" is defined for each device. In general, this parameter increases based on α (where $\alpha > 0$) after a device working in the ED mode receives an acknowledgement (ACK) signal, or after a device working in the VGW mode receives an ACK for a signal it has relayed; inversely, the parameter is used to decrease $k\alpha$ (with $k > 1$) when a device working in the VGW mode responds to a forwarding request. Here, the parameter k is used to control the speed at which a point is decreased through the product $k\alpha$.

Note that a VGW mode device receiving a negative-acknowledgement (NAK) signal or transmitting its own data does not affect the value of its point. Additionally, for a forward request, the point decreases only one time no matter how many retransmissions are required. A simple summary of this device management method indicating how a point is modified is shown in Table 1.

TABLE 1. Simple summary of the device management method.

Mode	Data source	ACK	NAK	Resp. of forward request
ED	own	$+\alpha$	0	-
VGW	own	0	0	-
VGW	others	$+\alpha$	0	$-k\alpha$

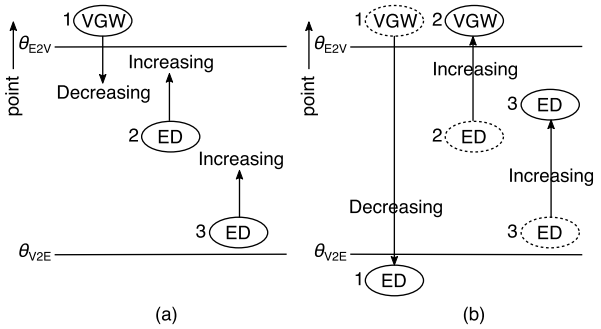

FIGURE 2. Illustration of the mode switching method with $\theta_{\mathrm{E2V},u,t} = \theta_{\mathrm{E2V}}, \theta_{\mathrm{V2E},u,t} = \theta_{\mathrm{V2E}}, \forall u, t$.

B. MODE SWITCHING METHOD

In our study, we consider two time-varying threshold values $\theta_{\mathrm{E2V},u,t}$ and $\theta_{\mathrm{V2E},u,t}$, with $\theta_{\mathrm{E2V},u,t} > \theta_{\mathrm{V2E},u,t}$, for each device to control which mode the device u should work in. Basically, at the instant t, an ED mode device u will switch to the VGW mode if its current point exceeds $\theta_{\mathrm{E2V},u,t}$; correspondingly, a device working in the VGW mode should switch to ED mode if its point value is less than $\theta_{\mathrm{V2E},u,t}$. After a mode switch takes place, the device informs the gateway of its current mode.

For clarity Fig. 2 provides an illustration of the mode switching method with fixed $\theta_{\mathrm{E2V},u,t} = \theta_{\mathrm{E2V}}$ and $\theta_{\mathrm{V2E},u,t} = \theta_{\mathrm{V2E}}$ for all u and t. Specifically, in Fig. 2(a), device 1, which is working in the VGW mode, relays signals that are transmitted from other devices and decreases its point by $(k-1)\alpha$ after accurately demodulating the signals. On the other hand, devices 2 and 3, which are working in the ED mode, send data and increase their point values by α after their data are accurately demodulated. As a result, the more data device 1 relays and the more data devices 2 or 3 send, the more their points decrease and increase, respectively.

Once the point of device 1 falls below the given threshold value θ_{V2E}, as shown in Fig. 2(b), device 1 switches to the ED mode and will begin to increase its point value. Similarly, once the points of devices 2 and 3 exceed their given threshold value of θ_{E2V}, they switch to VGW mode and will begin to decrease their points based on the quantity of data they relay. In the case of Fig. 2(b), device 2 will switch to the VGW mode and provide data relaying, while device 3 will continue in ED mode for some time.

It is noteworthy that as mentioned in Sect. I-C, two thresholds $\theta_{\mathrm{E2V},u,t}$ and $\theta_{\mathrm{V2E},u,t}$ can be customized for each device u and each time instant t based on given conditions such as whether an external power supply is available. For instance, a device u can set a smaller value of $\theta_{\mathrm{V2E},u,t}$ if it is supplied by an external power source at instant t. In this case, the device remains in VGW mode and continuously provides relay services regardless of the local battery power remaining. Inversely, a device u' with poor battery performance can set a larger $\theta_{\mathrm{E2V},u',t}$ at the same instant t to remain in ED mode to conserve power. Thus, flexible configurations of the two thresholds that consider individual device characteristics can be easily handled in practice.

C. PATH DETERMINATION ALGORITHM

Determination of the transmission path is considered as a unicast routing [34] with multi-hop, in which a device can use other devices working in the VGW mode as relays to reach the gateway, such as the route from device 1 to the gateway through device 2 or 3 shown in Fig 1. To ensure that the proposed path determination algorithm can avoid being affected by the rapid change of an instantaneous channel condition (i.e., small-scale fading) and to reduce computational complexity, we configure the routing process in the proposal so that it is mainly dominated by the large-scale fading attenuation among devices, which consists of path loss and spatially correlated shadowing.

Thus, the received signal on the ith equipment[6] transmitted from the jth equipment at time instant t is written as

$$\boldsymbol{y}_{i,j}(t) = g_{i,j}^{\frac{1}{2}} p_{\mathrm{t},j}^{\frac{1}{2}} \boldsymbol{x}_{i,j}(t) + \boldsymbol{n}_i(t), \tag{1}$$

where $\boldsymbol{x}_{i,j} \in \mathbb{C}$ for the link between i and j, where $i, j \in \mathcal{E} := \{1, \{u+1\}_{u\in\mathcal{U}}\}$ is the modulated signal vector drawn from a zero-mean Gaussian codebook with unit average power. $\boldsymbol{n}_i \in \mathbb{C}$ is the additive white Gaussian noise at equipment i following a complex normal distribution with zero mean and N_0 power per Hertz. $p_{\mathrm{t},j}$ is the transmit power scaling factor on equipment j. We use $g_{i,j} \in \mathbb{R}$ to represent the large-scale fading between i and j, and assume that this fading is known for the network and is time-invariant. Furthermore, we define a channel gain matrix for all equipment as $\boldsymbol{G} = (g_{i,j}) \in \mathbb{R}^{|\mathcal{E}|\times|\mathcal{E}|}$, where i (or j) $= 1$ and i (or j) $= u+1$, and $u \in \mathcal{U}$ are the indexes of the gateway and uth device, respectively. The problem in this subsection is thereby formulated to finding a suitable transmission route beginning from an arbitrary j (except $j = 1$), and ending at $i = 1$ (i.e., the gateway) with the help of $\boldsymbol{G}$.

It is noteworthy that, based on the above assumptions, the large-scale fading coefficients only change when equipment considerably changes its geographical location. Therefore, typically, for static or low-speed IoT transmission scenarios, we can consider that the wireless channels are constant during a channel coherence time [33], i.e., estimates of the channel gain matrix at gateway and relevant calculations for path determination are valid in this time interval. For a particular scenario where high-speed mobility plays an important role, due to equipment location changes significantly during the channel coherence time and small-scale fading

[6]In the present study, devices and gateway are called "equipment" in general.

has to be also taken into consideration, improvement on the accuracy of channel estimation becomes an unavoidable and common challenge. In future, based on varying channel conditions, more advanced path determination algorithms will be proposed to handle the mobility issues for our study.

In general, currently, various routing algorithms are used for the purpose of deciding which route an incoming data packet should follow to reach its destination efficiently [34]. To conserve space, this study applies the well-known and widely used Dijkstra's algorithm described in [35] to find the "shortest" paths between a source device and a gateway, and originally the algorithm is denoted by

$$\Lambda_{\theta,\phi} = \mathbb{D}\left(\boldsymbol{M}, \theta, \phi\right), \tag{2}$$

where $\Lambda_{\theta,\phi}$ denotes the outputted paths starting at $\phi \in \mathcal{E}$ and ending at $\theta \in \mathcal{E}$. Here, $\mathbb{D}$ represents Dijkstra's algorithm and its source code is open code. The matrix $\boldsymbol{M}$ is the input graph. Obviously, the aforementioned word "shortest" is not suitable for signal propagation. However, because passing through a wireless channel with larger gain g usually means lower cost regarding power consumption, we reasonably regard the channel with the largest gain as the "shortest" path. Mathematically, the matrix $\boldsymbol{G}^{-1\circ}$ thus can be used as the input graph $\boldsymbol{M}$ for Dijkstra's algorithm.

To properly fit the proposed mode switching method described in the above subsection to our network, there are several constraints applied to the matrix $\boldsymbol{G}^{-1\circ}$ that need to be clarified. First, to ensure that at each time instant the source and destination represent different equipment in the algorithm, we set the diagonal values in $\boldsymbol{G}^{-1\circ}$ to be larger, and a modified version of matrix $\boldsymbol{G}^{-1\circ}$ applying this constraint is thus obtained as

$$\boldsymbol{C}_1 \leftarrow \left[\boldsymbol{G}^{-1\circ}\right]_{i,i} = \rho, \tag{3}$$

where $i \in \mathcal{E}$, and $\rho > 0$ is a huge value. As a example, we can use the "inf" or "NaN" functions to define ρ in Matlab [36].

Second, considering that only the devices which are working in VGW mode can relay signals and can be further selected as valid hop nodes in Dijkstra's algorithm, we format another matrix constrained by the above description as

$$\boldsymbol{C}_2 \leftarrow \left[\boldsymbol{G}^{-1\circ}\right]_{\{1+u\}_{u\in\mathcal{U}_{\mathrm{ED}}}\backslash\phi,\,\mathcal{E}} = \rho, \tag{4}$$

$$\boldsymbol{C}_2 \leftarrow [\boldsymbol{C}_2]_{\mathcal{E},\,\{1+u\}_{u\in\mathcal{U}_{\mathrm{ED}}}\backslash\phi} = \rho, \tag{5}$$

where $\mathcal{U}_{\mathrm{ED}} \subseteq \mathcal{U}$ represents a device collection, and all devices in this collection are working in ED mode. Note that because an ED mode device can be a source node in the algorithm, we exclude the source ϕ from collection $\{1+u\}_{u\in\mathcal{U}_{\mathrm{ED}}}$, and the collection $\mathcal{U}_{\mathrm{ED}}$ is obtained by applying the proposed device management method and mode switching method.

Finally, to reduce the probability of data loss as far as possible during the a multi-hop transmission, the channel gain g of each path in the outputted $\Lambda_{\theta,\phi}$ is strongly expected to be larger than the gain of a single hop in the star topology system. Based on this fact, we generate a matrix with this final constraint as

$$\boldsymbol{C}_3 \leftarrow \left[\boldsymbol{G}^{-1\circ}\right]_{\hat{i},\hat{j}} = \rho, \tag{6}$$

where

$$\hat{i}, \hat{j} = \arg_{i,j\in\mathcal{E}}\left(g_{i,j}^{-1} > g_{\theta,\phi}^{-1}\right). \tag{7}$$

Consequently, according to (2), the outputted routing paths $\Lambda_{\theta,\phi}$ can be found by solving

$$\Lambda_{\theta,\phi} = \mathbb{D}\left(\frac{1}{3}\sum_{q=1}^{3}\boldsymbol{C}_q, \theta, \phi\right). \tag{8}$$

For better understanding, we conclude the proposed path determination algorithm in **Algorithm** 1.

Algorithm 1 Path Determination Algorithm

Input: $\mathcal{E}, \mathcal{U}_{\mathrm{ED}}, g_{i,j}\forall i,j \in \mathcal{E}, \theta \in \mathcal{E}, \phi \in \mathcal{E}, \rho$;
Output: $\Lambda_{\theta,\phi}$;
Initialization: $\boldsymbol{G} = (g_{i,j}) \in \mathbb{R}^{|\mathcal{E}|\times|\mathcal{E}|}$;
$\%\mathcal{E} := \{1, \{u+1\}_{u\in\mathcal{U}}\}$, $\mathcal{U}$ is device collection, $\mathcal{U}_{\mathrm{ED}}$ is ED mode worked device collection, $g_{i,j}$ is the large-scale fading between i and j, ϕ is the starting device, θ is the end device, ρ is a large positive number, $\Lambda_{\theta,\phi}$ is the outputted path;
%Modification of $\boldsymbol{G}^{-1\circ}$ for constraint 1;
$\boldsymbol{G}_{\mathrm{inv}} = \boldsymbol{G}^{-1\circ}$;
foreach $i \in \mathcal{E}$ **do**
  $[\boldsymbol{G}_{\mathrm{inv}}]_{i,i} = \rho$;
end
$\boldsymbol{C}_1 = \boldsymbol{G}_{\mathrm{inv}}$;
%Modification of $\boldsymbol{G}^{-1\circ}$ for constraint 2;
$\boldsymbol{G}_{\mathrm{inv}} = \boldsymbol{G}^{-1\circ}$;
$\mathcal{E}' = \{1+u\}_{u\in\mathcal{U}_{\mathrm{ED}}}\backslash\phi$;
foreach $i \in \mathcal{E}'$ **do**
  $[\boldsymbol{G}_{\mathrm{inv}}]_{i,\,\mathcal{E}} = \rho$;
end
foreach $i \in \mathcal{E}'$ **do**
  $[\boldsymbol{G}_{\mathrm{inv}}]_{\mathcal{E},\,i} = \rho$;
end
$\boldsymbol{C}_2 = \boldsymbol{G}_{\mathrm{inv}}$;
%Modification of $\boldsymbol{G}^{-1\circ}$ for constraint 3;
$\boldsymbol{G}_{\mathrm{inv}} = \boldsymbol{G}^{-1\circ}$;
foreach $i,j \in \mathcal{E}$ **do**
  if $g_{i,j}^{-1} > g_{\theta,\phi}^{-1}$ **then**
    $[\boldsymbol{G}_{\mathrm{inv}}]_{i,j} = \rho$;
  end
end
$\boldsymbol{C}_3 = \boldsymbol{G}_{\mathrm{inv}}$;
%Output path, $\mathbb{D}(\cdot)$ is the Dijkstra's algorithm [35];
$\Lambda_{\theta,\phi} = \mathbb{D}\left(\frac{1}{3}\left(\boldsymbol{C}_1 + \boldsymbol{C}_2 + \boldsymbol{C}_3\right), \theta, \phi\right)$;

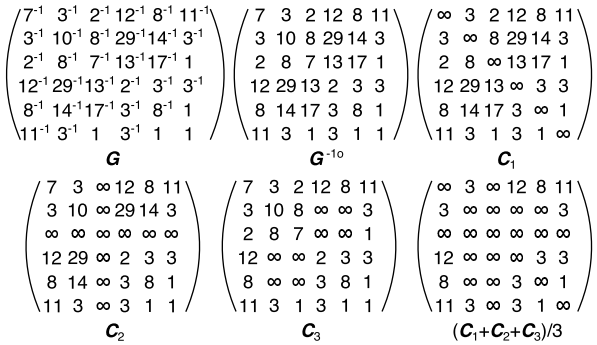

FIGURE 3. Examples of matrices G and $G^{-1\circ}$, and their variations C_1, C_2, and C_3 with destination $\theta = 1$, source $\phi = 4$, $\mathcal{U}_{\mathrm{ED}} = \{2, 3\}$, and $\rho = \infty$.

As an example, Fig. 3 shows the matrices $\boldsymbol{G}$ and $\boldsymbol{G}^{-1\circ}$ and their variations $\boldsymbol{C}_1$, $\boldsymbol{C}_2$, and $\boldsymbol{C}_3$ considering the aforementioned three constraints with destination $\theta = 1$ (i.e., the gateway), source $\phi = 4$, $\mathcal{U}_{\mathrm{ED}} = \{2, 3\}$, and $\rho = \infty$. The matrix inputted to the algorithm $\mathbb{D}$ is also indicated by the last matrix in the figure. In this case, the outputted path $\Lambda_{1,4}$ is $1 \leftarrow 2 \leftarrow 6 \leftarrow 4$, and the cost of this multi-hop routing is 9, which is lower than the cost of the single hop path $1 \leftarrow 4$.

III. CHANNEL MODELS AND ACCESS METHOD

In this section, to demonstrate the effectiveness of the proposal, we provide detailed descriptions of the wireless channel models and the access method employed in our simulations. The channel consists of several classic propagation models, and a suitable and effective access method is considered and included in our current study.

A. CHANNEL MODEL

Considering the traditional IoT transmission environments, we assume that devices and gateway are static or have low mobility. From a communications point of view, this assumption suggests and ensures that channel conditions around the equipment are mainly affected by the variation of large-scale fading and thus do not change rapidly. Commonly, the large-scale fading attenuation between equipment i and j, i.e., $g_{i,j}$, given in (1) can be further extended and written as

$$g_{i,j} = d_{i,j}^{-\zeta} \times 10^{0.1 s_{i,j}}, \tag{9}$$

where $d_{i,j}$ denotes the distance between equipment j and i in meters, and $s_{i,j}$ is the shadowing attenuation from j to i in decibels. The first term on the right-hand side of (9), i.e., $d_{i,j}^{-\zeta}$, is the path loss between two devices or a device and the gateway, and is usually modeled by a distance-dependent power function with base $d_{i,j}$ and exponent $-\zeta$ [37], [38].

The second term on the right-hand side of (9), i.e., $10^{0.1 s_{i,j}}$, represents the spatially correlated shadowing coefficient between equipment j and i, where $s_{i,j}$ $\forall i, j$ is a Gaussian random variable (RV) following a normal distribution with mean $\mu_{i,j}$ and variance $\sigma_{i,j}^2$. Previous experiments indicated that for the case when the gateway has the same height as the devices, shadowing auto-correlation and shadowing cross-correlation, i.e., the correlation between the RVs $s_{i,j}$ and $s_{i,j'}$ for $j \neq j'$, and the correlation between the RVs $s_{i,j}$ and $s_{i',j}$ for $i \neq i'$, both can be modeled via an exponential decay function [39].

Based on this fact and to reduce system complexity, we assume that gateways are basically higher than devices within a limited difference, and reciprocity applies to the shadowing process (i.e., $s_{i,j} = s_{j,i}$ $\forall i, j$). According to a method that originally is proposed in [39] and later adopted by [25], the coefficient of spatially correlated shadowing $s_{i,j}$ can thus be generated by the positions of equipment. Mathematically, $s_{i,j}$ is calculated by

$$s_{i,j} = \mu_{i,j} + \sigma_{i,j}\sqrt{\frac{2}{N_{\mathrm{c}}}}\sum_{n_{\mathrm{c}}=1}^{N_{\mathrm{c}}} \cos\Big(2\pi\big(f_{\mathrm{Th},n_{\mathrm{c}}} z_{\mathrm{h},j} + f_{\mathrm{Tv},n_{\mathrm{c}}} z_{\mathrm{v},j} + f_{\mathrm{Rh},n_{\mathrm{c}}} z_{\mathrm{h},i} + f_{\mathrm{Rv},n_{\mathrm{c}}} z_{\mathrm{v},i}\big) + \psi_{n_{\mathrm{c}}}\Big), \tag{10}$$

where N_{c} represents the number of sinusoids for the generation of correlated shadowing. $z_{\mathrm{h},i}$ and $z_{\mathrm{v},i}$ denote the horizontal and vertical position coordinates of equipment i, respectively. $\psi_{n_{\mathrm{c}}}$ represents uniformly distributed RV in the range of $[0, 2\pi)$.

The coefficients $f_{\mathrm{Th},n_{\mathrm{c}}}$, $f_{\mathrm{Tv},n_{\mathrm{c}}}$, $f_{\mathrm{Rh},n_{\mathrm{c}}}$, and $f_{\mathrm{Rv},n_{\mathrm{c}}}$ in (10) are frequency RVs for shadowing generation, and can be calculated by

$$\begin{cases} f_{\mathrm{Th},n_{\mathrm{c}}} = f_{n_{\mathrm{c}}} \cos\left(\psi_{\mathrm{T},n_{\mathrm{c}}}\right), f_{\mathrm{Tv},n_{\mathrm{c}}} = f_{n_{\mathrm{c}}} \sin\left(\psi_{\mathrm{T},n_{\mathrm{c}}}\right) \\ f_{\mathrm{Rh},n_{\mathrm{c}}} = f_{n_{\mathrm{c}}} \cos\left(\psi_{\mathrm{R},n_{\mathrm{c}}}\right), f_{\mathrm{Rv},n_{\mathrm{c}}} = f_{n_{\mathrm{c}}} \sin\left(\psi_{\mathrm{R},n_{\mathrm{c}}}\right), \end{cases} \tag{11}$$

where $f_{n_{\mathrm{c}}}$ is further expressed as

$$f_{n_{\mathrm{c}}} = \frac{\ln 2}{2\pi d_{\mathrm{cor}}}\sqrt{\frac{1}{\left(1-\omega_{n_{\mathrm{c}}}\right)^2} - 1}, \tag{12}$$

where d_{cor} denotes the shadowing correlation distance in meters [40], and $\omega_{n_{\mathrm{c}}}$ is a RV uniformly distributed over the range of [0, 1]. The coefficients $\psi_{\mathrm{T},n_{\mathrm{c}}}$ and $\psi_{\mathrm{R},n_{\mathrm{c}}}$ in (11) both are uniformly distributed RVs over $[0, 2\pi)$.

B. CHANNEL ACCESS METHOD

In practice, various channel access methods have been widely adopted in LPWA systems. For instance, a simple protocol named slotted Additive Links On-line Hawaii Area (ALOHA) was introduced in LoRaWANs as a random medium access method [41], [42]. The core of this protocol is to decrease data collisions by retransmitting after a specified wait time. Another well-known access method worth mentioning is carrier-sense multiple access with collision avoidance (CSMA/CA), which is beneficial in Wi-SUNs [7] and wireless local area networks (WLANs). In this access method, carrier sensing is used, while devices attempt to avoid collisions by beginning transmission only after the communication channel is sensed to be free [43], [44].

In general, although the channel access methods employed in LoRaWAN and Wi-SUN are quite different, their primary

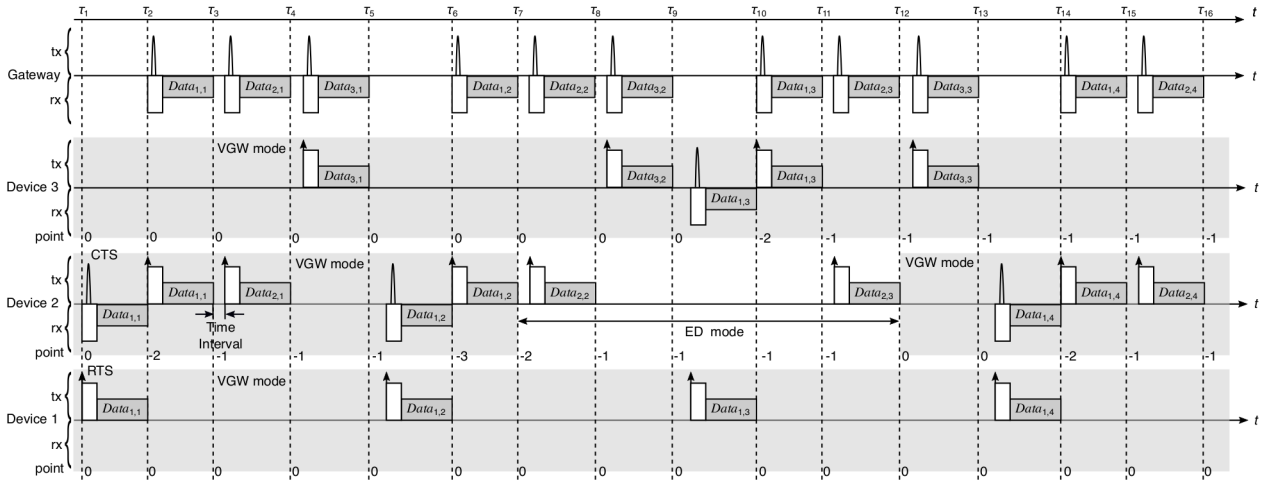

FIGURE 4. Example of data transmission with use of $|\mathcal{U}| = 3$, $\alpha = 1$, $k = 2$, $\theta_{\mathrm{E2V},u,t} = 0$, and $\theta_{\mathrm{V2E},u,t} = -2$ for all u and t. Points are initialized to zero and VGW is the default mode for all devices.

purpose is to reduce the probability of signal collisions as far as possible and thereby improve system throughput. To better focus on evaluating the proposed networking approach presented in Sect. II, we overlook the effects of channel access methods and consider a simplified transmission scenario for all related network deployments, in which no signal collisions are assumed.

More specifically, we force the uth device with $u \in \mathcal{U}$ to send its first data packet to the gateway following the route defined by $\Lambda_{1,u+1}$ and other devices are kept silent. Once the transmission of this packet reaches the gateway, a time interval ϵ is used for all devices to refresh their current mode (ED or VGW) according to the proposed device management and mode switching methods. Thereafter, a routing result $\Lambda_{1,u'+1}$ for device $u' = u + 1$ is outputted by the path determination algorithm, and the u'th device then sends its first data packet to the gateway following this route. After the first data packets of $|\mathcal{U}|$ devices are transported, the second, third, and additional packets are continuously sent by all devices in the same manner described above.

Note that in the present access method, when a packet error is detected at an arbitrary receiver in a given transmission route, retransmission is requested from the corresponding transmitter. If retransmission fails many times and reaches a maximum number, the packet has to be dropped. All devices then refresh their modes, and the next device is allowed to send its packet.

Fig. 4, shows an example of data transmission using the proposal based on the Wi-SUN technique with $\mathcal{U} = \{1, 2, 3\}$, $\alpha = 1$, $k = 2$, $\theta_{\mathrm{E2V},u,t} = 0$, and $\theta_{\mathrm{V2E},u,t} = -2$ for all $u \in \mathcal{U}$ and t. We use $Data_{u,n}$ to represent the nth data packet sent by the uth device to the gateway, set VGW as the default mode, and initialize the point as zero for all devices. Details at time instant t for these devices are explained as follows:

- at τ_1, after route $\Lambda_{1,2} = 1 \leftarrow 3 \leftarrow 2$ (where "1", "2", and "3" denote the gateway, device 1, and device 2, respectively) is found, device 1 requests to send (RTS) its first data packet $Data_{1,1}$ to device 2 and waits to receive a clear to send (CTS) signal;
- at τ_2, after the request for sending $Data_{1,1}$ is acknowledged, device 2 decreases its point to -2 according to TABLE 1, receives $Data_{1,1}$, and begins to relay it to the gateway. Note that because the transmission of $Data_{1,1}$ is not complete, mode switching is not activated;
- at τ_3, once $Data_{1,1}$ is successfully received at the gateway, device 2 updates its point to -1. After waiting a time interval ϵ for mode switching and path determination, device 2 starts to send its first packet $Data_{2,1}$ to the gateway following the assumed route $\Lambda_{1,3} = 1 \leftarrow 3$;
- at τ_4, although $Data_{2,1}$ is received by the gateway, device 2 keeps its point as -1 because of the middle rule in TABLE 1. After waiting a time interval ϵ, device 3 begins to send its first packet $Data_{3,1}$ to the gateway following the assumed route $\Lambda_{1,4} = 1 \leftarrow 4$;
- at τ_5, similar to τ_4, the gateway receives the packet $Data_{3,1}$ and device 3 keeps its point as 0. After waiting a time interval ϵ, device 1 starts to send its second packet $Data_{1,2}$ to device 2 following the route $\Lambda_{1,2}$;
- at τ_6, similar to τ_2, after the request for sending $Data_{1,2}$ is acknowledged, device 2 decreases its point to -3, receives the $Data_{1,2}$, and begins to relay it to the gateway;
- at τ_7, when $Data_{1,2}$ is received at the gateway, device 2 increases its point to -2. Because $\theta_{\mathrm{V2E},u,t} = -2$, device 2 switches its mode to ED during the time interval ϵ, and starts to send its second packet $Data_{2,2}$ following the route $\Lambda_{1,3}$;
- at τ_8, after $Data_{2,2}$ is received at the gateway, device 2 which is working in ED mode, increases its point to -1;
- at τ_9, similar to τ_5, the gateway receives the packet $Data_{3,2}$ and device 3 keeps its point as 0. After waiting a time interval ϵ, device 1 starts to send packet $Data_{1,3}$

to device 3 following the different assumed route of $\Lambda'_{1,2} = 1 \leftarrow 4 \leftarrow 2$, noting that device 2 cannot relay data while operating in the ED mode;

- at τ_{10}, after the request for sending $Data_{1,3}$ is acknowledged, device 3 decreases its point to -2 according to TABLE 1, receives the $Data_{1,3}$, and begins to relay it to the gateway;
- at τ_{11}, because $Data_{1,3}$ is successfully received at the gateway, device 3 increases its point to -1. After waiting a time interval ϵ, device 2 starts to send packet $Data_{2,3}$ to the gateway following the route $\Lambda_{1,3}$;
- at τ_{12}, because device 2 is working in ED mode, when the transmission of $Data_{2,3}$ is complete, device 2 increases its point to 0 and switches mode to VGW;
- at τ_{13}, the gateway receives the packet $Data_{3,3}$ and device 3 keeps its point as -1. After waiting a time interval ϵ, device 1 starts to send packet $Data_{1,4}$ to device 2 following the route $\Lambda_{1,2}$;
- τ_{14}, τ_{15}, and τ_{16} are the same as τ_2, τ_3, and τ_4, respectively.

IV. SIMULATION PARAMETERS AND RESULTS

To analyze and evaluate the proposed networking approach presented in Sect. II, we demonstrate a series of data transfers using computer simulations based on star and mesh topologies as well as the proposal. In the current study, original data generated by all devices is attenuated through wireless channels which are modeled in the first subsection of Sect. III, and channels are accessed following the given channel access method introduced in the second subsection of Sect. III. After all data packets are transferred, we evaluate and analyze system throughputs, energy consumption, and other statistical properties for all of the network setups, and finally discuss some key findings.

A. SIMULATION PARAMETERS

In our simulations, a homogeneous[7] area with length R_{len} and width R_{wid} is considered. As shown in Fig. 5, a gateway is deployed at the origin of the coordinate system and $|\mathcal{U}|$ devices are uniformly distributed in the coverage area. With consideration that Wi-SUN is one of the most popular LPWA technologies in Japan, uplink transmission performed in Wi-SUNs is our major objective, and packet forwarding is not supported in star topology based systems but can be adopted in mesh topology networks or in the proposal.

The compliant standard for Wi-SUN is IEEE 802.15.4g and we employ Gaussian frequency shift keying (GFSK) as the frequency modulation scheme. To generate GFSK signals, we set modulation order and index which represent the size of symbol alphabet and the ratio of the bandwidth occupied around the carrier equal to 2 and 1, respectively. The bandwidth time product which is defined as the product of bandwidth and symbol time for the Gaussian pulse shape is set to 0.5 as a common value in Wi-SUN systems [7]. The detailed simulation parameters are listed in Table 2.

[7]When describing a material or system, the term "homogeneous" indicates having the same properties at every point in space; in other words, being uniform, without irregularities.

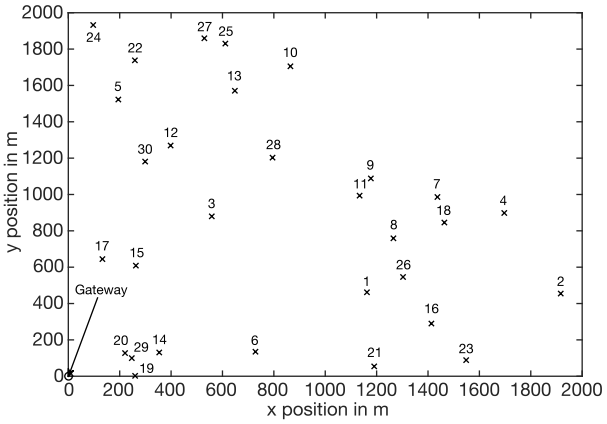

FIGURE 5. Deployment of gateway and devices for the considered simulation parameters. The number in the range of 1 to 30 denotes the index of a device.

TABLE 2. Simulation parameters.

Parameters	Values
Length of coverage area	$R_{\text{len}} = 2000$ m
Width of coverage area	$R_{\text{wid}} = 2000$ m
Path loss exponent	$\zeta = 4$
Mean of shadowing	$\mu_{i,j} = 0, \forall i, j$ [26]
Variance of shadowing	$\sigma^2_{i,j} = 9.6, \forall i, j$ [26]
Number of sinusoids for shadowing	$N_c = 300$
Shadowing correlation distance	$d_{\text{cor}} = 20$ m [40]
Thermal noise	-174 dBm/Hz
Compliant standard	IEEE 802.15.4g
Modulation scheme	GFSK
Modulation order	2
Modulation index	1
Bandwidth time product	0.5
Number of samples	8
Symbol rate	10^5 per second
Transmit power for each device	ranges from -10 to 15 in dBm
Number of gateways	1
Number of devices	$\|\mathcal{U}\| = 30$
Number of packets for each device	200
Packet length	800 bits
Number of retransmissions	5
Parameters α and k in proposal	$\alpha = 1, k = 2$
Threshold value $\theta_{\text{E2V},u,t}$	$\theta_{\text{E2V},u,t} = \theta_{\text{E2V}} = 0\ \forall u, t$
Threshold value $\theta_{\text{V2E},u,t}$	$\theta_{\text{V2E},u,t} = \theta_{\text{V2E}} < \theta_{\text{E2V}}\ \forall u, t$
Time interval	$\epsilon = 0$
Initial point of each device	0
Default mode for all devices	VGW

B. SIMULATION RESULTS

Figure 6 shows a comparison of system throughputs versus device transmit power calculated for the star, mesh, and the proposed networking approaches. Although the two threshold values $\theta_{\text{E2V},u,t}$ and $\theta_{\text{V2E},u,t}$ in the proposal can be dynamically set for each device in practice, to reasonably reduce the computational complexity of the simulations without loss of generality, for all of devices and arbitrary time instants, we fix the threshold $\theta_{\text{E2V},u,t}$ to $\theta_{\text{E2V}} = 0$, and assign $\theta_{\text{V2E}} = -2, -200, -400, -800, -1200$ to $\theta_{\text{V2E},u,t}$, respectively.

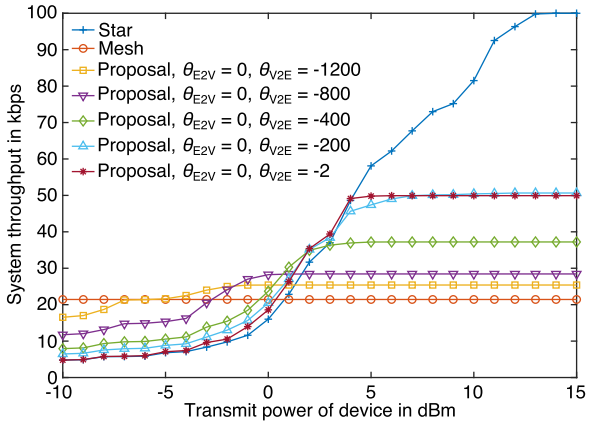

FIGURE 6. Comparison of system throughputs versus device transmit power calculated using star, mesh, and the proposed network topologies.

This figure indicates that three completely different throughput representations exist across the entire transmit power range. Specifically, in the case where the transmit power of each device is below to -4 dBm, the mesh topology method exhibited the best throughput performance; inversely, higher throughput can be achieved by the star topology network corresponding to the case in which the transmit power of each device is greater than 4 dBm. Interestingly, in the range between -4 dBm and 4 dBm, although the proposed networking method with various threshold settings demonstrated different throughput curves, a set of threshold parameters θ_{E2V} and θ_{V2E} that reaches the highest throughput among the network topologies in this transmit power range can always be found.

One of the major reasons why the throughput in the star topology network is inferior to that in the mesh network within the lower transmit power range is the large number of packet losses caused by the lower signal strength at the receiver. In this situation, the received signal strength is significantly affected by a poor communication environment and/or longer average access distance.

In addition, since shorter average access distance caused by the creation of multiple relay transmissions, packet loss has not been significantly observed in the mesh network within this lower transmit power range. In contrast, providing greater transmit power or better channel conditions cannot considerably improve the throughput in the mesh setup, because a number of relay operations calculated by the path determination algorithm must be performed, and packet delivery time is then extended because of these relays. Consequently, mesh topology achieves constant result throughout, even with change in transmit power.

On the other hand, by setting ED or VGW modes at each device and switching them based on the related thresholds, the proposal can be considered as a partially connected and dynamically changing mesh topology, which can take advantage of both the star and the traditional mesh systems, thereby resulting in an improvement in throughput across the entire transmit power range.

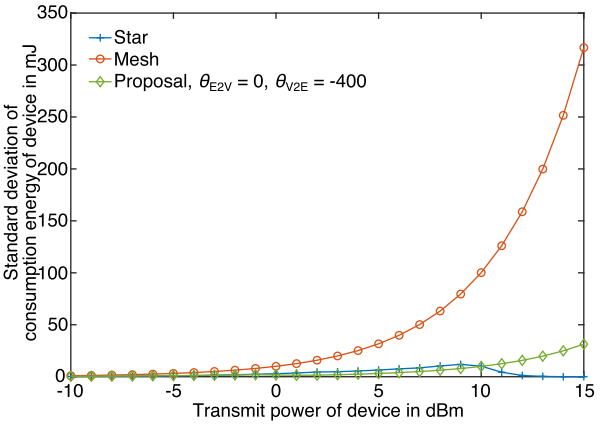

(a) Standard deviation of device consumption energy

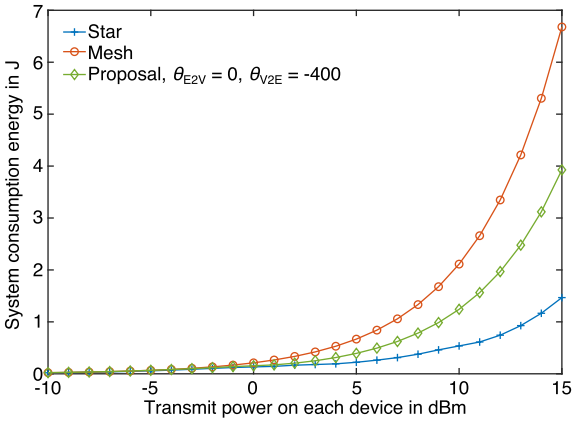

(b) System consumption energy

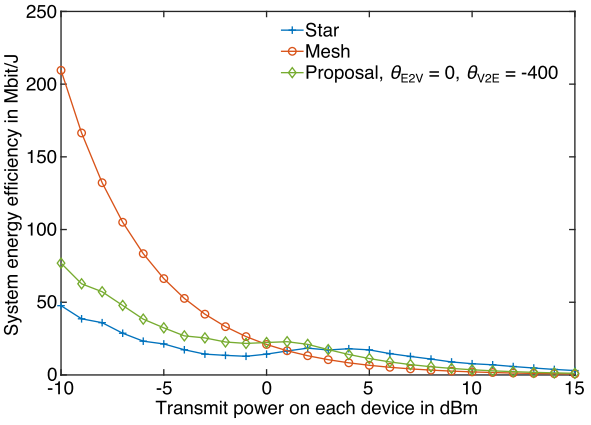

(c) System EE

FIGURE 7. Comparison of different transmission characteristics calculated using star, mesh, and the proposed network topologies for a given device transmit power.

To further evaluate the proposal from the viewpoint of energy cost, Figs. 7(a), (b), and (c), show the standard deviations for device consumption energy, system consumption energy, and system energy efficiency (EE) calculated for the star, mesh, and proposed networking approaches, respectively. To reduce computational cost and with a consideration of that gateways are commonly connected with external

power supplies, in the current study, we assume that the consumed energy can approximately be calculated as the product of transmit power and packet delivery time. The system EE is then defined as a ratio of system delivered bits and system consumption energy. For brevity, we focus on $\theta_{\mathrm{E2V}} = 0$ and $\theta_{\mathrm{V2E}} = -400$ threshold values for the proposal across the entire transmit power range same as in Fig. 6.

The subfigure (a) indicates that the energy consumption of devices in the traditional mesh system has the greatest standard deviation. This result verifies that compared to the star topology network, the mesh setup improves throughput performance by consistently using devices which have good channel conditions to provide data forwarding and hence consume more energy as relay nodes. In contrast, the proposal drives these inactive devices in the data forwarding process to relay packets and provides some opportunities for the active devices to rest; consequently, the proposal balances the consumed energy among all devices to the greatest extent possible.

Furthermore, the star network has the similar standard deviation as the proposal in the transmit power ranged from -10 to 10 dBm. However, for large transmit power, since all of devices can successfully deliver their packets without retransmission, the consumed energy for sending these packets on each device is identical, and thereby the standard deviation of the star system approaches zero with the increasing of device transmit power.

The total consumed energy of the three systems shown in subfigure (b) supports the above analysis and provides similar results as subfigure (a). In addition, the system EE of the three networking approaches versus device transmit power is shown in subfigure (c). The results further indicate that the lower the transmit power (and/or the worse the channel conditions), the greater the system EE of the mesh topology system; on the contrary, the higher the transmit power (and/or the better the channel conditions), the greater the system EE of the star topology system. Regarding the proposal, we can consider it as a dynamic network setup that bridges the gap between the star and the traditional mesh setups.

Thereafter, we attempted to clarify the relationships among the three networking approaches mentioned in the present study. To accomplish this, the curve of a customized coefficient $\eta_{\theta_{\mathrm{E2V}},\theta_{\mathrm{V2E}}}$ ranging from 0 to 1 versus the difference between thresholds θ_{E2V} and θ_{V2E}, i.e., $\theta_{\mathrm{E2V}} - \theta_{\mathrm{V2E}}$, is shown in Fig. 8. The coefficient $\eta_{\theta_{\mathrm{E2V}},\theta_{\mathrm{V2E}}}$ is defined by the formula

$$\eta_{\theta_{\mathrm{E2V}},\theta_{\mathrm{V2E}}} = 1 - \frac{\beta^{\mathrm{pro\&mesh}}_{\theta_{\mathrm{E2V}},\theta_{\mathrm{V2E}}}}{\beta^{\mathrm{star\&mesh}}}, \tag{13}$$

where $\beta^{\mathrm{pro\&mesh}}_{\theta_{\mathrm{E2V}},\theta_{\mathrm{V2E}}}$ is the square root of the second instant of the differences between the throughputs of the proposed and the mesh systems across the entire transmit power range with parameters θ_{E2V} and θ_{V2E}. Similarly, $\beta^{\mathrm{star\&mesh}}$ is the square root of the second instant of the differences between the throughputs of the star and mesh systems. According to the above description, the transmission performance of the proposal will be similar to that of the traditional mesh setup as $\eta_{\theta_{\mathrm{E2V}},\theta_{\mathrm{V2E}}}$ increases, and finally produces the same outputs as the outputs of the mesh topology system when $\eta_{\theta_{\mathrm{E2V}},\theta_{\mathrm{V2E}}} = 1$. Inversely, the outputs will be similar to those of the star topology system with decreasing $\eta_{\theta_{\mathrm{E2V}},\theta_{\mathrm{V2E}}}$. Mathematically, $\eta_{\theta_{\mathrm{E2V}},\theta_{\mathrm{V2E}}}$ can be calculated as

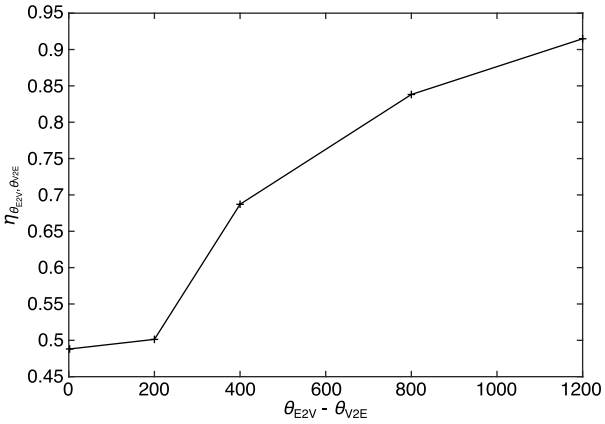

FIGURE 8. Relationship between a customized coefficient $\eta_{\theta_{\mathrm{E2V}},\theta_{\mathrm{V2E}}}$ and the difference between thresholds θ_{E2V} and θ_{V2E} used to compare the similarity of the proposed, mesh, and star systems.

$$\eta_{\theta_{\mathrm{E2V}},\theta_{\mathrm{V2E}}} = 1 - \frac{\sqrt{\sum_{p_{\mathrm{t}}} \left(c^{\mathrm{pro}}_{p_{\mathrm{t}},\theta_{\mathrm{E2V}},\theta_{\mathrm{V2E}}} - c^{\mathrm{mesh}}_{p_{\mathrm{t}}} \right)^2}}{\sqrt{\sum_{p_{\mathrm{t}}} \left(c^{\mathrm{star}}_{p_{\mathrm{t}}} - c^{\mathrm{mesh}}_{p_{\mathrm{t}}} \right)^2}}, \tag{14}$$

where $c^{\mathrm{pro}}_{p_{\mathrm{t}}}$, $c^{\mathrm{mesh}}_{p_{\mathrm{t}}}$, and $c^{\mathrm{star}}_{p_{\mathrm{t}}}$ denote the throughputs obtained by the proposed, mesh, and star networking approaches with device transmit power equal to p_{t}, respectively.

Figure 8 indicates that the coefficient $\eta_{\theta_{\mathrm{E2V}},\theta_{\mathrm{V2E}}}$ increases with increasing $\theta_{\mathrm{E2V}} - \theta_{\mathrm{V2E}}$, and approaches unity as $\theta_{\mathrm{E2V}} - \theta_{\mathrm{V2E}}$ approaches infinity. The result suggests that the greater the difference between θ_{E2V} and θ_{V2E} is, the more similar the transmission performances of the proposal and mesh configuration will be. In fact, the gap between the threshold values θ_{E2V} and θ_{V2E} in the proposed mode-switching method indirectly represents a switching period in which the device switches its mode. A longer period usually means that a device takes more time when determining whether to remain in its current mode. Because the VGW mode (allowing data forwarding) is the initial mode and the two threshold values are time-invariant for all devices in the current simulations, introducing an unlimited time period, i.e., $\theta_{\mathrm{E2V}} - \theta_{\mathrm{V2E}} \to \infty$, in the proposal causes the arrangement of the equipment to become the traditional mesh topology, thereby yielding the same transmission performance.

For a dynamic switching period, i.e., $\theta_{\mathrm{E2V},u,t} - \theta_{\mathrm{V2E},u,t}$ that varies over device index u and time instant t, the changes of throughput and other transmission performances become more complex, and are difficult to measure without more specific and practical parameter settings. However, because a partially connected and dynamically changing mesh setup

is one of the fundamental features of the proposed networking approach and thus will not change, similar results to those described in the previous statements are predicted. To perform additional analyses and evaluations considering the dynamic switching period, flexible configurations in these thresholds that consider individual device characteristics will be addressed based on experiments in our future work.

V. DISCUSSION

In practice, both the star and traditional mesh systems have several limitations that are difficult to overcome. For instance, (a) using the star topology to create a network using devices with a built-in power supply will result in insufficient power, or propagation attenuation will be significant; or (b) using mesh topology in the case where each device has larger transmit power capability or where channel conditions are good, neither (a) nor (b) is practical. Actually, dynamically deciding on whether to adopt a star or mesh network topology is difficult for operators, in particular when having to monitor the battery power remaining in thousands of devices in real time and dynamically estimating the channel status. Consumers who do not have a background in communication will be at a loss to understand the complexities involved.

According to the results presented in Sect. IV, the proposed networking approach can adopt the advantages of both star and mesh based systems, enable dynamic changes in network configuration, and finally ensure that its transmission performance is comparable to that of other topologies in most cases. By adopting the proposal, the decision process regarding network topology can be skipped, and thus this IoT technique can be widely accepted and more easily used to the benefit of general consumers.

Moreover, the core of the proposal is based on the concept of decentralization. The working mode (ED or VGW) can be decided and managed autonomously by a device according to the device's state rather than by a gateway. For instance, assuming that energy for a battery-powered device is also derived from external sources such as direct current power, solar power, or thermal energy, then by increasing the gap between the two thresholds and switching to VGW mode, a device can continuously provide relay services to improve system performances without requiring permission from the gateway, or when a device is low on power, by decreasing the gap and switching to ED mode, the device can complete its data transfer with the help of other devices. Basically, decisions by the gateway are limited, and each device in the proposal plays an important role and acts in intelligent fashion.

Other valuable subjects should be investigated and solved in the near future. For instance, in the current study, a suitable channel access method is introduced in Sect. III-B to reduce the computational cost for simulations. Actually, slotted ALOHA, CSMA/CA, and other existing access methods have been adopted and used in LoRaWAN, Wi-SUN FAN, and other LPWA systems. In future work, we will evaluate those common access methods for our proposed system and perform various experiments to evaluate the proposal in practice.

VI. CONCLUSION

To actively develop and promote IoT related techniques, this study proposed a dynamic and non-centric networking approach using virtual gateway platforms, and evaluated it based on LPWA techniques through comparisons using the traditional star and mesh networks. In our approach, we first presented a device management method for each local device, in which two working modes, ED and VGW, are controlled to indicate whether or not the device provides relay services, and an internal parameter named the ''point'' is defined to manage mode switching by considering the device's current state, such as battery power remaining. We thereafter proposed a mode switching method where two time-varying threshold values are configured and help each local device to switch between the two modes based on its point value. Finally, a path determination algorithm was selected and applied to find routes for data transmission with or without using the devices playing the role of a VGW. Computer simulation results indicated that the proposed networking approach can use the advantages of both traditional star and mesh systems, enables dynamic and non-centric changes in network configuration, and finally ensures that, in most cases, the transmission performance is comparable or better than that of other network setups.

REFERENCES

[1] Z. Qin, F. Y. Li, G. Y. Li, J. A. McCann, and Q. Ni, "Low-power wide-area networks for sustainable IoT," *IEEE Wireless Commun.*, vol. 26, no. 3, pp. 140–145, Jun. 2019.
[2] S. Popli, R. K. Jha, and S. Jain, "A survey on energy efficient narrowband Internet of Things (NBIoT): Architecture, application and challenges," *IEEE Access*, vol. 7, pp. 16739–16776, 2019.
[3] H. Wang and A. O. Fapojuwo, "A survey of enabling technologies of low power and long range machine-to-machine communications," *IEEE Commun. Surveys Tuts.*, vol. 19, no. 4, pp. 2621–2639, 1st Quart., 2017.
[4] Q. M. Qadir, T. A. Rashid, N. K. Al-Salihi, B. Ismael, A. A. Kist, and Z. Zhang, "Low power wide area networks: A survey of enabling technologies, applications and interoperability needs," *IEEE Access*, 2018, pp. 77454–77473, 2018.
[5] S. Andreev, O. Galinina, A. Pyattaev, M. Gerasimenko, T. Tirronen, J. Torsner, J. Sachs, M. Dohler, and Y. Koucheryavy, "Understanding the IoT connectivity landscape: A contemporary M2M radio technology roadmap," *IEEE Commun. Mag.*, vol. 53, no. 9, pp. 32–40, Sep. 2015.
[6] M. Saari, A. M. bin Baharudin, P. Sillberg, S. Hyrynsalmi, and W. Yan, "LoRa—A survey of recent research trends," in *Proc. 41st Int. Conv. Inf. Commun. Technol., Electron. Microelectron. (MIPRO)*, Opatija, Croatia, May 2018, pp. 872–877.
[7] H. Harada, K. Mizutani, J. Fujiwara, K. Mochizuki, K. Obata, and R. Okumura, "IEEE 802.15.4g based wi-sun communication systems," *IEICE Trans. Commun.*, vol. E100-B, pp. 1032–1043, Jul. 2017.
[8] A. Augustin, J. Yi, T. Clausen, and W. M. Townsley, "A study of LoRa: Long range & low power networks for the Internet of Things," *Sensors*, vol. 16, pp. 1–18, Sep. 2016.
[9] M. Liu, J. Yang, and G. Gui, "DSF-noma: UAV-assisted emergency communication technology in a heterogeneous Internet of Things," *IEEE Internet Things J.*, vol. 6, no. 3, pp. 5508–5519, Jun. 2019.
[10] Y. Xu, G. Li, Y. Yang, M. Liu, and G. Gui, "Robust resource allocation and power splitting in swipt enabled heterogeneous networks: A robust minimax approach," *IEEE Internet Things J.*, vol. 6, no. 6, pp. 10799–10811, Dec. 2019, doi: 10.1109/jiot.2019.2941897.
[11] *SX1301 Datasheet v2.01*, Semtech Corporation, Camarillo, CA, USA, Jun. 2014.

[12] L. Feltrin, C. Buratti, E. Vinciarelli, R. De Bonis, and R. Verdone, "Lorawan: Evaluation of link- and system-level performance," *IEEE Internet Things J.*, vol. 5, no. 3, pp. 2249–2258, Jun. 2018.
[13] V. A. Dambal, S. Mohadikar, A. Kumbhar, and I. Guvenc, "Improving LoRa signal coverage in urban and sub-urban environments with uavs," in *Proc. Int. Workshop Antenna Technol. (iWAT)*, Miami, FL, USA, Mar. 2019, pp. 210–213.
[14] C. Orfanidis, L. M. Feeney, M. Jacobsson, and P. Gunningberg, "Investigating interference between LoRa and IEEE 802.15.4g networks," in *Proc. IEEE 13th Int. Conf. Wireless Mobile Comput., Netw. Commun. (WiMob)*, Rome, Italy, Oct. 2017, pp. 1–8.
[15] J. Xu, J. Yao, L. Wang, Z. Ming, K. Wu, and L. Chen, "Narrowband Internet of Things: Evolutions, technologies, and open issues," *IEEE Internet Things J.*, vol. 5, no. 3, pp. 1449–1462, Jun. 2018.
[16] M. Centenaro, L. Vangelista, A. Zanella, and M. Zorzi, "Long-range communications in unlicensed bands: The rising stars in the IoT and smart city scenarios," *IEEE Wireless Commun.*, vol. 23, no. 5, pp. 60–67, Oct. 2016.
[17] A. Hoeller, R. D. Souza, and O. L. A. López, H. Alves, M. de Noronha Neto, and G. Brante, "Analysis and performance optimization of LoRa networks with time and antenna diversity," *IEEE Access*, vol. 6, pp. 32820–32829, Jul. 2018.
[18] F. Van den Abeele, J. Haxhibeqiri, I. Moerman, and J. Hoebeke, "Scalability analysis of large-scale LoRaWAN networks in ns-3," *IEEE Internet Things J.*, vol. 4, no. 6, pp. 2186–2198, Dec. 2017.
[19] M. Slabicki, G. Premsankar, and M. Di Francesco, "Adaptive configuration of LoRa networks for dense IoT deployments," in *Proc. IEEE/IFIP NOMS*, Apr. 2018, pp. 1–9.
[20] M. N. Ochoa, A. Guizar, M. Maman, and A. Duda, "Evaluating LoRa energy efficiency for adaptive networks: From star to mesh topologies," in *Proc. IEEE WiMob*, Oct. 2017, pp. 1–8.
[21] H.-C. Lee and K.-H. Ke, "Monitoring of large-area IoT sensors using a LoRa wireless mesh network system: Design and evaluation," *IEEE Trans. Instrum. Meas.*, vol. 67, no. 9, pp. 2177–2187, Sep. 2018.
[22] C.-H. Liao, G. Zhu, D. Kuwabara, M. Suzuki, and H. Morikawa, "Multi-hop LoRa networks enabled by concurrent transmission," *IEEE Access*, vol. 5, pp. 21430–21446, 2017.
[23] Z. Zhou, K. Ota, M. Dong, and C. Xu, "Energy-efficient matching for resource allocation in D2D enabled cellular networks," *IEEE Trans. Veh. Technol.*, vol. 66, no. 6, pp. 5256–5268, Jun. 2017.
[24] Y. Wang, Y. He, C. Xu, Z. Zhou, S. Mumtaz, J. Rodriguez, and H. Pervaiz, "Joint rate control and power allocation for low-latency reliable D2D-based relay network," *EURASIP J. Wireless Commun. Netw.*, vol. 2019, p. 111, May 2019.
[25] O. Zhao, L. Shan, W.-S. Liao, M. G. Kibria, H.-B. Li, K. Ishizu, and F. Kojima, "A device-centric clustering approach for large-scale distributed antenna systems using user cooperation," *IEICE Trans. Commun.*, vol. E102-B, no. 2, pp. 359–372, Feb. 2019.
[26] L. Shan, O. Zhao, K. Temma, K. Hattori, F. Kojima, and F. Adachi, "Evaluation of machine learnable bandwidth allocation strategy for user cooperative traffic forwarding," *IEEE Access*, vol. 7, pp. 85213–85225, 2019.
[27] L. Shan, O. Zhao, K. Temma, K. Hattori, H. B. Li, F. Kojima, and F. Adachi, "Experimental evaluation of energy efficiency for virtual small-cell networks using smartphone test-bed," in *Proc. 23rd Asia–Pacific Conf. Commun. (APCC)*, Perth, Australia, Dec. 2017, pp. 1–5.
[28] N. Ayub and V. Rakocevic, "Fair battery power consumption algorithms for relay nodes in rural wireless networks," in *Proc. Int. Conf. Wireless Netw. Mobile Commun. (WINCOM)*, Rabat, Morocco, Nov. 2017, pp. 1–6.
[29] *Decentralization: A Sampling of Definitions*, United Nations Develop. Programme, New York, NY, USA, pp. 11–12, Oct. 1999.
[30] S. H. Boko, "Decentralization: Definitions, theories and debate" in *Decentralization Reform Africa*. Boston, MA, USA: Springer, 2002.
[31] B. Cao, Y. Li, L. Zhang, L. Zhang, S. Mumtaz, Z. Zhou, and M. Peng, "When Internet of Things meets blockchain: Challenges in distributed consensus," *IEEE Netw.*, to be published.
[32] T. J. Grant, "Network Topology," in *Command and Control: Organization, Operation, and Evolution*, 1st ed. Hershey, PA, USA: IGI Global, May 2014.
[33] F. A. P. de Figueiredo, F. A. C. M. Cardoso, I. Moerman, and G. Fraidenraich, "Channel estimation for massive mimo tdd systems assuming pilot contamination and flat fading," *EURASIP J. Wireless Commun. Netw.*, vol. 2018, Jun. 2017, Art. no. 14.
[34] V. Rabarijaona, F. Kojima, H. Harada, and C. Powell, "Enabling layer 2 routing in ieee std 802.15.4 networks with IEEE std 802.15.10," *IEEE Commun. Standards Mag.*, vol. 1, no. 1, pp. 44–49, Mar. 2017.
[35] K. Mehlhorn and P. Sanders, *Algorithms Data Structures: The Basic Toolbox*. Springer, 2008.
[36] H. Moore, *MATLAB for Engineers: Global Edition*, 5th ed. New York, NY, USA: Pearson, 2018.
[37] O. Zhao and H. Murata, "A study on dynamic clustering for large-scale multi-user MIMO distributed antenna systems with spatial correlation," *IEICE Trans. Commun.*, vol. E99-B, no. 4, pp. 928–938, Apr. 2016.
[38] O. Zhao and H. Murata, "Sum rate analysis of MU-MISO systems with ZF beamforming over composite fading channels," *IEICE Trans. Fundamentals*, vols. E98–A, pp. 558–568, Feb. 2015.
[39] Z. Wang, E. K. Tameh, and A. R. Nix, "Joint shadowing process in urban peer-to-peer radio channels," *IEEE Trans. Veh. Technol.*, vol. 57, no. 1, pp. 52–64, Jan. 2008.
[40] O. Zhao and H. Murata, "Sum-rate analysis for centralized and distributed antenna systems with spatial correlation and inter-cell interference," *IEICE Trans. Commun.*, vol. E98-B, no. 3, pp. 449–455, Mar. 2015.
[41] D. Magrin, M. Centenaro, and L. Vangelista, "Performance evaluation of LoRa networks in a smart city scenario," in *Proc. IEEE Int. Conf. Commun. (ICC)*, May 2017, pp. 1–7.
[42] S.-Y. Wang, Y.-R. Chen, T.-Y. Chen, C.-H. Chang, Y.-H. Cheng, C.-C. Hsu, and Y.-B. Lin, "Performance of LoRa-based IoT applications on campus," in *Proc. IEEE 86th Veh. Technol. Conf. (VTC-Fall)*, Toronto, ON, Canada, Sep. 2017, pp. 1–6.
[43] *LoRaWAN Specification V1.0*, LoRa Alliance, Jan. 2015.
[44] *IEEE Standard for Information Technology–Telecommunications and Information Exchange Between Systems Local and Metropolitan Area Networks–Specific Requirements Part 11: Wireless LAN Medium Access Control (MAC) and Physical Layer (PHY) Specifications*, IEEE Standard 802.11-2012 (Revision of IEEE Standard 802.11-2007), Mar. 2012, pp. 1–2793.

OU ZHAO received the B.E. degree in electronics and communication engineering from the Nanjing University of Posts and Telecommunications (NJUPT), China, in 2005, and the M.E. and Ph.D. degrees in electronic engineering from the Graduate School of Informatics, Kyoto University, Kyoto, Japan, in 2014 and 2016, respectively. He is currently a Researcher working with the Wireless Networks Research Center, National Institute of Information and Communications Technology (NICT). His major research interests include resource allocation, wireless signal processing and its hardware implementation, machine learning, and big data analytics. He received the Young Researcher's Encouragement Award from the Japan Chapter of the IEEE Vehicular Technology Society (VTS), in 2013.

WEI-SHUN LIAO received the B.S., M.S., and Ph.D. degrees in electrical engineering and wireless communications from National Taiwan University (NTU), Taipei, Taiwan, in 2000, 2002, and 2014, respectively. From 2002 to 2007, he worked with BenQ Corporation to develop technologies involving eNB, cellular phones, multimedia transmission, and digital homes. From 2014 to 2015, he worked as a Postdoctoral Researcher with the Graduate Institute of Communication Engineering (GICE), NTU. In 2016, he joined the National Institute of Information and Communications Technology (NICT), Yokosuka, Kanagawa, Japan, where he is currently a Researcher with the Wireless System Laboratory (WSL), Wireless Networks Research Center. His research interests include wireless communications, cross-layer algorithm design, wireless signal processing, and homogeneous networks.

KENTARO ISHIZU received the Ph.D. degree in computer science from Kyushu University, Japan, in 2005. Since then, he has been working with the National Institute of Information and Communications Technology (NICT), Yokosuka, Japan. He has been involved in Research and Development on heterogeneous wireless networks, cognitive radio systems, and TV White Space systems. One of the developed systems was sent to the disaster area of the great earthquake that took place in eastern Japan on March 2011 and used to recover the damaged network access environment. He has been leading NICT's TV White Space trials at various locations in the world. He has also been involved with wide area network international standardizations, including the IEEE 1900.4, 802.11, and the IEEE 802.21. He is currently managing the Research and Development efforts on future mobile wireless communication systems.

FUMIHIDE KOJIMA received the B.E., M.E., and D.E. degrees in electrical communications engineering from Osaka University, Osaka, Japan, in 1996, 1997, and 1999, respectively. He is currently the Director of the Wireless Systems Laboratory, Wireless Networks Research Center, National Institute of Information and Communications Technology, Yokosuka, Japan. In 1999, he joined the Communications Research Laboratory, Ministry of Posts and Telecommunications, where he has been engaged in research on various topics, such as intelligent transportation systems, radio-over-fiber multimedia transmissions, mobile ad hoc emergency networks, wireless grid systems, and medium access control protocols for communications systems.